Broadband imaging optical fiber based on multicomponent glasses for endoscopy in the VIS-NIR band

Mariusz Mrózek,[*,2] Dariusz Pysz,[2] Rafał Kasztelanic,[2] Adam Wojciechowski,[1] and Ryszard Buczyński[2]

[1]*Institute of Physics, Jagiellonian University, Lojasiewicza 11, 30-348 Krakow, Poland*
[2]*Department of Physics, University of Warsaw, Pasteura 5, 02-093 Warsaw, Poland*

Received March 12, 2026; accepted June 30, 2026; published June 30, 2026

Abstract—The development of multimodal diagnostic techniques requires advanced tools for *in vivo* imaging. This paper presents the design, fabrication, and optical characterization of a broadband multicore optical fiber, adapted to operate in the visible (VIS) and near-infrared (NIR) wavelength ranges. A fiber structure comprising more than 13,000 cores within a 400 μm-diameter cross-section was fabricated from multicomponent glasses using the stack-and-draw technique. Based on measurements and analytical calculations, the fiber's numerical aperture (NA) was determined to be 0.53. Its transmission properties were characterized in the 400−1100 nm spectral range. The experimental results reveal a high image transmittance of up to 74.5% and an average attenuation of 1.40 dB, demonstrating the potential of this structure for ultra-thin fluorescent and coherent endoscopes.

The dynamic progress in the field of minimally invasive medical diagnostics, including the development of confocal endomicroscopy, fluorescence diagnostics, and optical coherence tomography (OCT) [1], imposes rigorous demands on the miniaturization of imaging tools. Conventional optical systems based on rigid lens arrays (so-called rod endoscopes) are being gradually replaced by flexible microprobes. The essential transmission medium of such a system is an image guide: a coherent microfiber bundle or a single multicore microstructured fiber (MCF) [2].

A fundamental engineering challenge in the design of broadband optical fibers is to effectively reduce evanescent coupling (optical crosstalk) between densely packed cores [3]. This phenomenon, which degrades the contrast of the transmitted image, increases with wavelength, a factor that has previously significantly limited imaging resolution in the near-infrared (NIR) range. The solution to these problems has been the use of soft, multicomponent glasses (silicate, lead, and borosilicate), characterized by a wide transmission window and the ability to control the refractive index precisely [4]. A proper selection of two thermally matched soft glasses enables the construction of imaging optical fibers with extremely high refractive-index contrast [5].

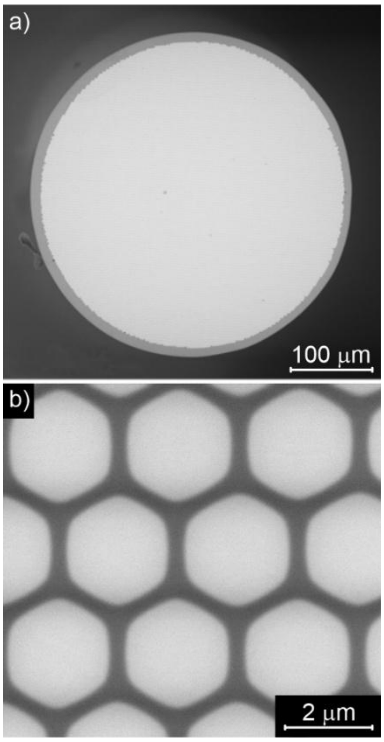

Fig. 1: a) Photo of the optical fiber end face, b) close-up of individual pixels. The average pixel size is 2.5 μm.

This significantly reduces crosstalk between neighboring cores, and allows reducing individual core diameter in the imaging fiber, resulting in high-resolution, high-contrast imaging across a broad spectral range [6,7]. Based on these results, we discuss the properties of an optimized, next-generation optical imaging fiber designed to operate over a broad transmission band from 400 to 1100 nm.

The presented imaging optical fiber was fabricated using the classical stack-and-draw method, the effectiveness of which for soft glasses has already been demonstrated in previous articles [8]. Since we target in-vivo application,

* E-mail: mariusz.mrozek@uj.edu.pl

high refractive index lead silicate glasses were not used in the fabrication process, because lead compounds are not favorable for biomedical applications.

In the first stage of the fabrication process, a structured rod is fabricated using the "rod in the tube" method, with a high-refractive-index glass rod and a low-refractive-index glass capillary. The core rods were made of zirconium silicate glass, which combines a high refractive index (n_D = 1.609) without lead (PbO) content. The capillary was formed from optimized soda-lime silicate glass doped with alkali metal oxides, characterized by a lower refractive index (n_D = 1.520). The ratio of rod to capillary diameters determines the ratio of core to lattice pitch in the final imaging optical fiber. To obtain a high-density imaging bundle, we used a 10 mm-diameter rod and a 12 mm outer-diameter, 1.6 mm-thick capillary. We place the rod into the capillary, then draw it at the fiber-drawing tower to integrate and scale down. As a result, the structured rods with an outer diameter of 400 μm are developed.

In the next step of the fabrication process, a set of over 13,000 structured rods is manually placed inside a large-diameter capillary and arranged according to a hexagonal lattice to form the fiber preform. The structural preform was drawn onto a fiber-optic tower toward the final imaging fiber (Fig. 1).

A key aspect of materials engineering in this case was closely matching the rheological properties (viscosity curves) and thermal expansion coefficients of both glasses. This allows stable co-drawing of the structure on the fiber-optic tower and prevents stress cracking at the core-cladding interface during final cooling. The refractive index contrast (Δn) was set to 0.089 to ensure strong lightwave guidance even at wavelengths close to 1100 nm. This contrast allows for a high numerical aperture NA = 0.53. This translates directly into a wide lightwave acceptance angle. The full cone of view of the image fiber is approximately 64°, which enables highly efficient collection of the light signal from the examined materials.

The final outer diameter of the flexible imaging fiber is 400 μm. The effective diameter of a single core is estimated at 2.5 μm, with a lattice constant (pitch) of 2.9 μm, which corresponds to a hexagonal arrangement with the highest packing factor. Consequently, the cross-section fill factor reaches 55.4%, representing an optimal compromise between pixel density and the cladding thickness insulating the cores. Furthermore, analytically determined wave propagation parameters confirm that the individual cores operate in the multimode regime, stabilizing broadband transmission. The normalized frequency (V) is approximately 5.76 at 550 nm (propagating approximately 16 modes) and drops to 3.17 at 1000 nm (propagating approximately 5 modes).

Broadband spectrometric measurements were performed to determine the optical fiber's transmission characteristics. The intensity of the input beam I_{in} from a white light source supported by a halogen lamp and the output signal I_{out} after the fiber sample were recorded, which allowed the determination of the fiber's absolute wavelength transmittance and attenuation profile in the band from 400 nm to 1100 nm (Avantes AvaSpec-ULS2048 spectrometer).

As the recorded data demonstrate, the developed structure is characterized by high transmittance ranging from 56.8% to 74.5% in visible spectrum (Fig. 2).

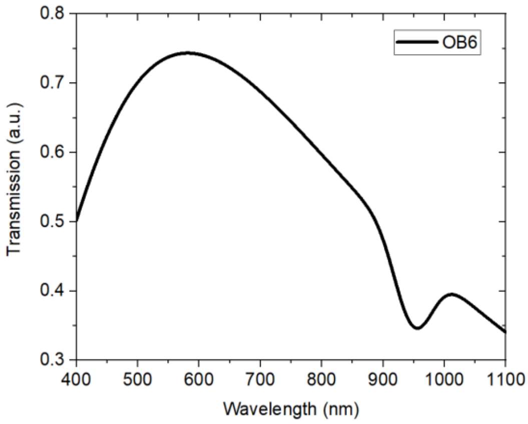

Fig. 2. Transmission spectrum from a 40 cm section of optical fiber.

Measurement results demonstrate good conduction of both shorter wavelengths in the visible light range (for a 450 nm wavelength, transmittance is 61.7%, and attenuation is approximately 1.32 dB) with a peak transmittance of 74.5% for 565 nm (losses on level 1.28 dB).

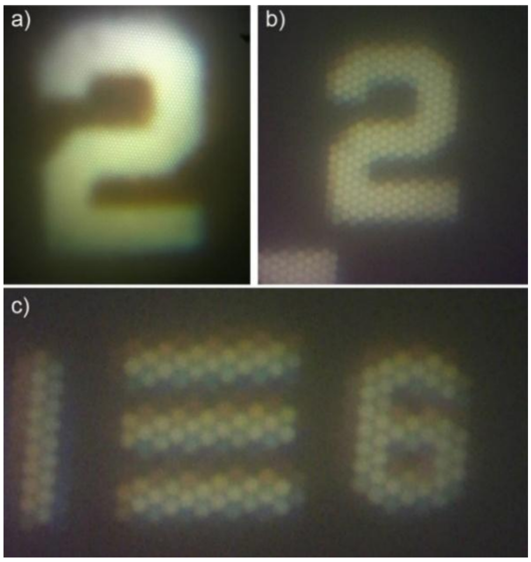

Fig. 3. Example of imaging of 1951 USAF Resolution Test Targets: a) line width 32 μm, b) line width 10 μm, c) line width 5 μm.

The average attenuation of the optical fiber determined in the tested transmission window is 1.40 dB. However, it is worth noting the occurrence of a local attenuation maximum around 950 nm, reaching a value of 2.45 dB. This effect results directly from the absorption resonances of hydroxyl (OH-) groups trapped in the matrix of multicomponent glass during its melting process, a typical phenomenon in this type of oxide materials [9].

To empirically evaluate the spatial resolution of the fabricated imaging fiber, tests were conducted using a standard 1951 USAF resolution test target. The transmitted images (Figure 3) demonstrate the fiber's ability to resolve fine details. Specifically, the system successfully resolves line pairs with widths of 32 µm, 10 µm, and down to 5 µm. This high resolution correlates well with the structural parameters of the fiber, namely the 2.5 µm core diameter and 2.9 µm pitch. This confirms that the low optical crosstalk between adjacent cores enables the high-contrast imaging necessary for precise diagnostics.

Further evaluation of the imaging quality was performed by transmitting a sinusoidal optical grating pattern through the fiber. Figure 4 illustrates the experimental intensity profiles compared to the ideal sinusoidal input for grating periods of 50 µm and 23 µm. The experimental data closely match the ideal curves, indicating excellent contrast transfer and minimal signal distortion. Although theoretical simulations suggest a full coupling length of approximately 1.8 mm between adjacent cores, the applied refractive index contrast of 0.089 effectively mitigates severe image degradation over typical short probe lengths. As a result, the multicore structure maintains sharp feature definition even at smaller spatial periods.

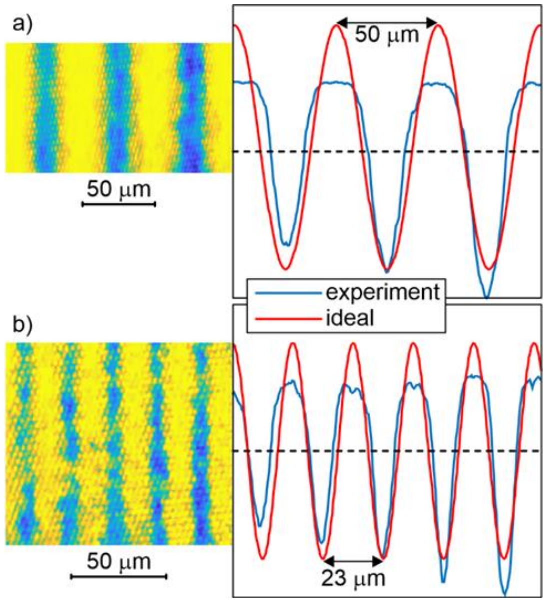

Fig. 4. Example of imaging sinusoidal grating: a) sinusoidal grid period 50 µm, b) sinusoidal grid period 23 µm.

This work demonstrated a technologically mature structure of a multicore imaging optical fiber made of soft glass. The achieved packing density of over 13,000 cores at a diameter of 400 µm enables the transmission of high-resolution images with an optimized cross-sectional fill factor of 55.4% and a high numerical aperture NA = 0.53. Numerical and experimental analysis of the transmission profile in the range from 400 to 1100 nm demonstrates very stable operation of the structure, characterized by a low average attenuation of 1.40 dB and transmittance of up to 74.5%. The designed imaging optical fibers provide a solid foundation for the construction of miniaturized endomicroscopic systems capable of simultaneous colorimetric tissue analysis (VIS) and multimodal imaging, potentially including spatially encoded infrared scanning.

This research was funded by the Medical Research Agency within the framework of the National Recovery and Resilience Plan, Project No. KPOD.07.07-IW.07-0212/24.

References

[1] D. Huang, E.A. Swanson, C.P. Lin, J.S. Schuman, W.G. Stinson, W. Chang, M.R. Hee, T. Flotte, K. Gregory, C.A. Puliafito, J.G. Fujimoto, Science 254(035), 1178 (1991). https://doi.org/10.1126/science.1957169

[2] W. Chen, L. Yuan, B. Zhang, Q. Yu, Z. Lian, Y. Pi, C. Shan, P.P. Shum, Photonics **11**, 270, (2024). https://doi.org/10.3390/photonics11030270

[3] J. Roper, *Advances in multicore optical fibres for endoscopy*, Doctoral Thesis 2016.

[4] R. Stępień, J. Cimek, D. Pysz, I. Kujawa, M. Klimczak, R. Buczyński, Opt. Eng. **53**(7), 071815 (2014). https://doi.org/10.1117/1.OE.53.7.071815

[5] J. Cimek, R. Stępień, G. Stepniewski, B. Siwicki, P. Stafiej, M. Klimczak, D. Pysz, R. Buczyński, Opt. Mat. **62**, 159 (2016). https://doi.org/10.1016/j.optmat.2016.09.061

[6] R. Stepien, J. Cimek, D. Pysz, I. Kujawa, P. Golebiewski, G. Stepniewski, K. Orlinski, R. Buczynski, R. Kasztelanic, Opt. Mat. Expr. **10**(8), 1891 (2020). https://doi.org/10.1364/OME.394918

[7] B. Morova, N. Bavili, Ö. Yaman, B. Yigit, M. Zeybel, M. Aydin, B. Dogan, R. Kasztelanic, D. Pysz, R. Buczynski, A. Kiraz, Opt. Expr. **27**(7), 9502 (2019). https://doi.org/10.1364/OE.27.009502

[8] D. Pysz, I. Kujawa, R. Stępień, M. Klimczak, A. Filipkowski, M. Franczyk, L. Kociszewski, J. Buźniak, K. Haraśny, R. Buczyński, Bull. Pol. Acad. Sci.-Tech. Sci. **62**(4), 667 (2014). https://doi.org/10.2478/bpasts-2014-0073

[9] V.G. Plotnichenko, V.O. Sokolov, E.M. Dianov, J. Non-Crystalline Solids **261**(1–3), 186 (2000). https://doi.org/10.1016/S0022-3093(99)00654-7